Study of the process $e^+e^- \to n\bar{n}$ at the VEPP-2000 e^+e^- collider with the SND detector

M. N. Achasov,[1,2] A. Yu. Barnyakov,[1,2] K. I. Beloborodov,[1,2] A. V. Berdyugin,[1,2] D. E. Berkaev,[1,2] A. G. Bogdanchikov,[1] A. A. Botov,[1] T. V. Dimova,[1,2] V. P. Druzhinin,[1,2] V. B. Golubev,[1,2] L. V. Kardapoltsev,[1,2] A. S. Kasaev,[1] A. G. Kharlamov,[1,2] A. N. Kirpotin,[1] I. A. Koop,[1–3] A. A. Korol,[1,2] S. V. Koshuba,[1,2] D. P. Kovrizhin,[1,2] A. S. Kupich,[1,2] K. A. Martin,[1,2] A. E. Obrazovsky,[1] E. V. Pakhtusova,[1] Yu. A. Rogovsky,[1,2] A. I. Senchenko,[1] S. I. Serednyakov,[1,2,*] Z. K. Silagadze,[1,2] Yu. M. Shatunov,[1,2] D. A. Shtol,[1] D. B. Shwartz,[1,2] A. N. Skrinsky,[1] I. K. Surin,[1] Yu. A. Tikhonov,[1,2] Yu. V. Usov,[1,2] and A. V. Vasiljev[1,2]

[1] *Budker Institute of Nuclear Physics, SB RAS, Novosibirsk 630090, Russia*
[2] *Novosibirsk State University, Novosibirsk 630090, Russia*
[3] *Novosibirsk State Technical University, Novosibirsk 630092, Russia*

(Received 15 October 2014; published 12 December 2014)

The process $e^+e^- \to n\bar{n}$ has been studied at the VEPP-2000 e^+e^- collider with the SND detector in the energy range from threshold up to 2 GeV. As a result of the experiment, the $e^+e^- \to n\bar{n}$ cross section and effective neutron form factor have been measured.

DOI: 10.1103/PhysRevD.90.112007 PACS numbers: 13.66.Bc, 13.40.Gp, 13.60.Rj, 14.20.Dh

I. INTRODUCTION

Nucleons (neutron and proton) have been the subject of theoretical and experimental studies for many decades. Their internal structure can be described in terms of the electromagnetic form factors, electric G_E and magnetic G_M, which are complex functions of the momentum transfer squared. To measure the nucleon timelike form factors, the reactions $e^+e^- \to p\bar{p}$, $n\bar{n}$ and $p\bar{p} \to e^+e^-$ are used. The $e^+e^- \to B\bar{B}$ cross section, where B is a spin-$1/2$ baryon with the mass m_B, is given by the following expression,

$$\frac{d\sigma}{d\Omega}(s,\theta) = \frac{\alpha^2\beta C}{4s}\left[|G_M(s)|^2(1+\cos^2\theta) + \frac{1}{\tau}|G_E(s)|^2\sin^2\theta\right], \tag{1}$$

where $s = 4E_b^2$, E_b is the beam energy, $\beta = \sqrt{1-4m_B^2/s}$, C is a factor taking into account the Coulomb interaction of the final baryons [$C = y/(1-e^{-y})$ with $y = \pi\alpha(1+\beta^2)/\beta$ for protons [1], and $C = 1$ for neutrons], $\tau = s/4m_B^2$, and θ is the baryon polar angle in the e^+e^- center-of-mass (c.m.) frame. The Coulomb interaction is significant at the energies not higher than 1 MeV above the threshold. At the threshold $|G_E| = |G_M|$. The total cross section has the following form:

$$\sigma(s) = \frac{4\pi\alpha^2\beta C}{3s}\left[|G_M(s)|^2 + \frac{1}{2\tau}|G_E(s)|^2\right]. \tag{2}$$

From the measurement of the total cross section the linear combination of squared form factors,

$$F(s)^2 = \frac{2\tau|G_M(s)|^2 + |G_E(s)|^2}{2\tau+1}, \tag{3}$$

can be determined. The function $F(s)$ is called the effective form factor. It is this function that is measured in most of e^+e^- and $p\bar{p}$ experiments. The $|G_E/G_M|$ ratio can be extracted from the analysis of the measured $\cos\theta$ distribution [see Eq. (1)].

The proton timelike form factor was studied in many experiments. The most precise measurement of the $e^+e^- \to p\bar{p}$ cross section in the energy region of interest was performed in the *BABAR* experiment [2]. For the ratio of the proton timelike form factors $|G_E/G_M|$ there are two measurements, *BABAR* [2] and PS170 [3], which contradict to each other. For neutron, the only measurement of the $e^+e^- \to n\bar{n}$ cross section was performed in the FENICE experiment [4], and there are no data on the $|G_E/G_M|$ ratio.

In this paper we present results on the neutron form factor in the c.m. energy range from threshold up to 2 GeV. The experiment has been carried out at the VEPP-2000 e^+e^- collider [5] with the SND detector [6] in Novosibirsk. The spherical neutral detector (SND) (Fig. 1) is a general-purpose nonmagnetic detector for a low-energy collider. It consists of a tracking system, a three-layer spherical NaI (Tl) electromagnetic calorimeter (EMC) and a muon detector. The experimental data used in this analysis were accumulated in 2011–2012 in the c.m. energy range 1.8–2.0 GeV. They correspond to an integrated luminosity of about 10 pb^{-1}. The typical collider luminosity near the nucleon threshold was about $5\times10^{30}\ \mathrm{cm}^{-2}\,\mathrm{s}^{-1}$.

II. EVENT SELECTION

The signature of $e^+e^- \to n\bar{n}$ events in the detector is atypical of e^+e^- annihilation processes. Both final

*seredn@inp.nsk.su

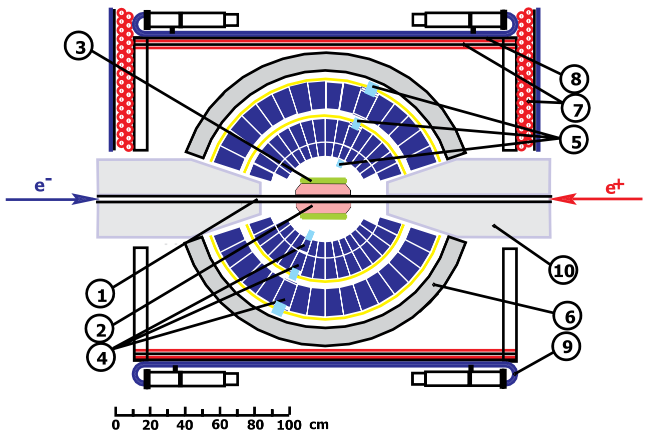

FIG. 1 (color online). Schematic view of the SND detector. The collider vacuum pipe (1) is surrounded by the tracking detector (2) based on a nine-layer drift chamber. The aerogel Cherenkov counter (3) provides K meson identification. The spherical electromagnetic calorimeter consists of 1680 NaI(Tl) crystals (4) with phototriode (5) readout. The muon detector (7)–(9) located after the iron absorber (6) provides muon identification and suppression of cosmic-ray background.

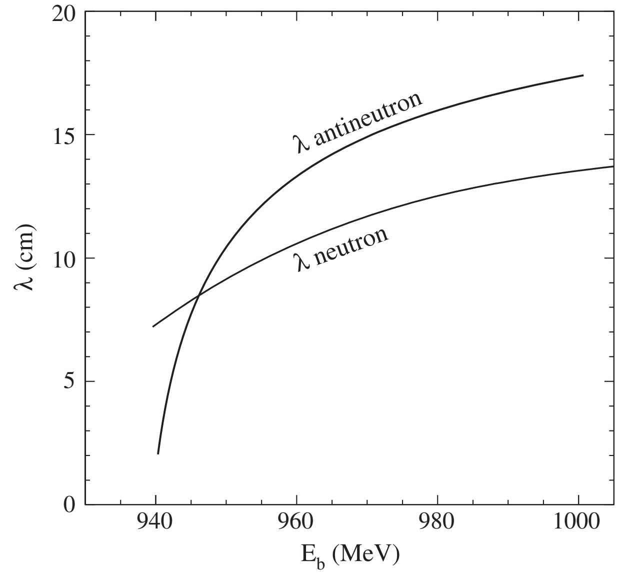

FIG. 2. Neutron and antineutron interaction lengths in NaI(Tl) as a function of the particle energy.

particles, neutron and antineutron, cross the tracking system without interaction and give signals deeply inside the EMC. So, a $n\bar{n}$ event does not contain "central" (originating from the e^+e^- interaction region) charged tracks and photons. The neutron interacting in the calorimeter material gives a low energy deposition, while the antineutron annihilates producing several pions with a total energy up to $2m_n$ GeV. Therefore, the total energy deposition in the EMC (E_{EMC}) for a $n\bar{n}$ event is usually large. But its distribution over the calorimeter crystals is strongly nonuniform; i.e., the event momentum calculated using energy depositions in the calorimeter crystals (P_{EMC}) significantly differs from zero. The $n\bar{n}$ event looks like several, often well separated, clusters (group of adjacent fired crystals) in the EMC. For most events, the event-reconstruction algorithm finds two or more photons. An event may also contain one or more not "central" charged tracks.

In the analyses of the $e^+e^- \to n\bar{n}$ process the value of the antineutron absorption length is of great significance. The energy dependence of neutron and antineutron absorption lengths in NaI(Tl) is shown in Fig. 2 [7]. It is seen that in the VEPP-2000 energy range the absorption lengths are much shorter than the effective calorimeter thickness, about 40 cm. This leads to a high (about 90% at 2 GeV) absorption efficiency of produced particles in the SND detector.

The selection of $n\bar{n}$ candidates is based on the event properties described above. We select events with at least two reconstructed photons. An event must have a large energy deposition ($E_{\mathrm{EMC}} > 950$ MeV) and a large unbalanced momentum in the EMC ($P_{\mathrm{EMC}} > 0.5E_b$). The condition on E_{EMC} provides full rejection of beam-background events and significant suppression of cosmic-ray background. To reduce the contribution from e^+e^- annihilation processes with charged particles we accept all events without tracks. Furthermore, an event is accepted if it has at most one track, and if in addition this track has $D > 0.6$ cm, where D is the distance between the charged particle track and the beam axis.

For further reduction of cosmic-ray background we use the veto from the muon system, the condition that the number of fired EMC layers in an event equals 3, the calorimeter energy $E_{\mathrm{EMC}} < 1500$ MeV and the requirement that there is no cosmic track in the calorimeter. The cosmic track is identified as a group of calorimeter crystal hits positioned along a straight line with $R_{\min} > 10$ cm, where $R_{\min}$ is a distance between the track and the detector centre.

To remove the residual background from not correctly reconstructed $e^+e^- \to e^+e^-(\gamma)$, $\gamma\gamma(\gamma)$ events we require that the fraction of the energy deposition in small-angle ($\theta < 36°$ or $\theta > 144°$) calorimeter crystals do not exceed 60%, and that the two most energetic clusters in the EMC are not back to back.

The remaining physical background is dominated by the processes with neutral particles (photons, π^0's, neutral kaons) in the final state, e.g., $e^+e^- \to \gamma\gamma(\gamma)$, $2\pi^0\gamma$, $K_SK_L2\pi^0$. To suppress the physical background we require that the most energetic photon in an event has the transverse energy profile not consistent with the profile expected for the electromagnetic shower [8], and the polar angle of the event momentum defined above be in the range $25° < \theta_{P_{\mathrm{EMC}}} < 155°$. The latter condition discriminates against multiphoton events containing extra photons emitted from the initial state at small angles. The physical background from the processes with charged particles is well suppressed by the track cuts described above.

After applying all the selection criteria, the initial number of events, about 10^9, recorded in the energy range 1.8–2.0 GeV is reduced to about 5×10^3.

III. DETECTION EFFICIENCY

The detection efficiency is determined using Monte Carlo (MC) simulation. Its energy dependence is shown in Fig. 3 separately for 2011 and 2012 data sets. At $E_b > 960$ MeV the efficiency weakly depends on energy and is about 18% above $E_b = 960$ MeV and decreases near the $n\bar{n}$ threshold to about 15%. The reason for this decrease is because the annihilation at lower $\bar{n}$ energy occurs near the center of the detector, and such central events are rejected by our selection cuts with a larger probability. A nonmonotonic behavior of the detection efficiency as a function of energy in 2011 and the difference between the efficiencies for 2011 and 2012 runs are due to variations of experimental conditions during the data taking period, in particular, due to dead calorimeter channels.

The detection efficiency is determined under the assumption that $|G_E| = |G_M|$, which is true at the threshold. In the *BABAR* experiment [2] a significant deviation of the $|G_E/G_M|$ ratio from unity was observed in the near-threshold region for the $e^+e^- \to p\bar{p}$ process. The ratio reaches 1.5. The deviation from unity is explained by effects of final state interaction [9]. A similar deviation is expected for neutron. The model dependence in the detection efficiency arises from limited detector acceptance. The detection efficiency as a function of $\cos\theta$ is shown in Fig. 4. The efficiency has a plateau in the range

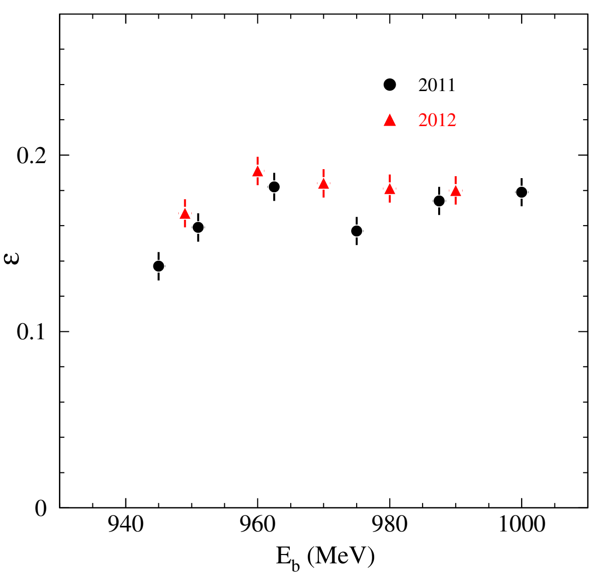

FIG. 3 (color online). The energy dependence of the detection efficiency for $e^+e^- \to n\bar{n}$ events determined using MC simulation. The filled circles show the efficiency for the 2011 data set, and the triangles for 2012.

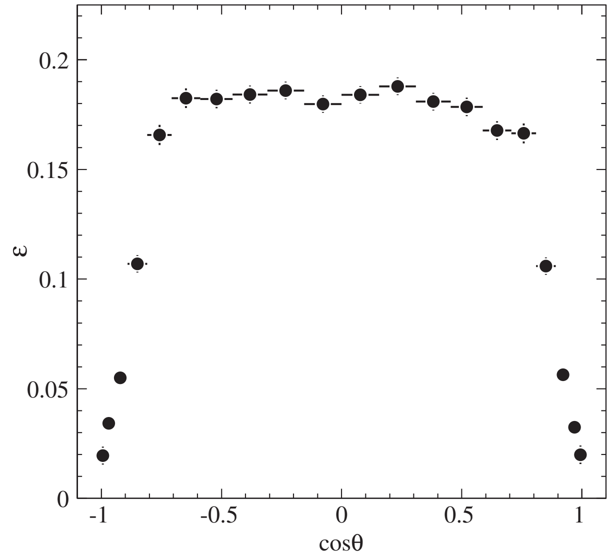

FIG. 4. The detection efficiency for $e^+e^- \to n\bar{n}$ events as a function of $\cos\theta$. The variable $\cos\theta$ bin size is used, corresponding to $\Delta\theta = 9°$.

$36° < \theta < 144°$, corresponding to $|\cos\theta| < 0.8$. The difference (3%) between the detection efficiencies determined with $|G_E/G_M| = 1.5$ and $|G_E/G_M| = 1$ is taken as an estimate of the model uncertainty.

Not quite perfect simulation of detector response for antineutrons may lead to systematic shift in the detection efficiency. In Fig. 5(a) we compare the distributions of the longitudinal position (number of EMC layer) of the crystal with maximum energy deposition in an $e^+e^- \to n\bar{n}$ event for data and simulation. The distribution for the data is obtained from the visible cross section for each of the three bins of Fig. 5(a), after removal of the background contamination with the procedure described in Sec. V. Since the data and simulated distributions are in agreement, we conclude that the probability of the antineutron absorption in the EMC is reproduced by the simulation reasonably well.

In Fig. 5(b) the distribution of the total energy deposition in the EMC is shown. Although the difference between the data and simulated distributions is not statistically significant, we interpret it as an indication of imperfect simulation. To reach better agreement, we shift the simulated spectrum to left by about 50 MeV. This leads to decrease of the detection efficiency by 10%. This value is taken as an estimate of the systematic uncertainty due to the condition on $E_{\rm EMC}$.

For other selection parameters (the total event momentum, the photon shower profile, the fraction of the energy deposited at small polar angles, etc.), we vary the cut boundaries over wide ranges and determine the variations of the measured cross section. The variations summed in quadrature are about 10%. A total systematic uncertainty in the detection efficiency including the model uncertainty and the uncertainty due to imperfect simulation of the detector response is estimated to be 14%.

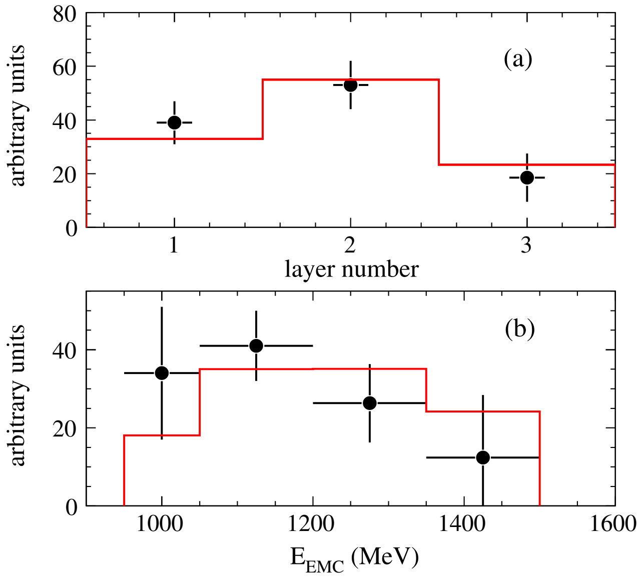

FIG. 5 (color online). (a) The distribution of the longitudinal position (number of EMC layer) of the crystal with maximum energy deposition in an $e^+e^- \to n\bar{n}$ event. (b) The distribution of the total energy deposition in the EMC for $e^+e^- \to n\bar{n}$ events. The points with error bars represent data. The histogram is the simulated distribution normalized to the area of the data distribution.

IV. ANGULAR DISTRIBUTION

The antineutron looks as a wide cluster or several clusters in the calorimeter. The polar angle of the calorimeter crystal with maximum energy deposition is used as an estimate of the antineutron polar angle. The distribution of the difference between the true and measured antineutron polar angles for simulated $n\bar{n}$ events is shown in Fig. 6. The RMS of this distribution is about 8°. About 70% of the reconstructed $n\bar{n}$ events are located within ±15° of the true antineutron direction.

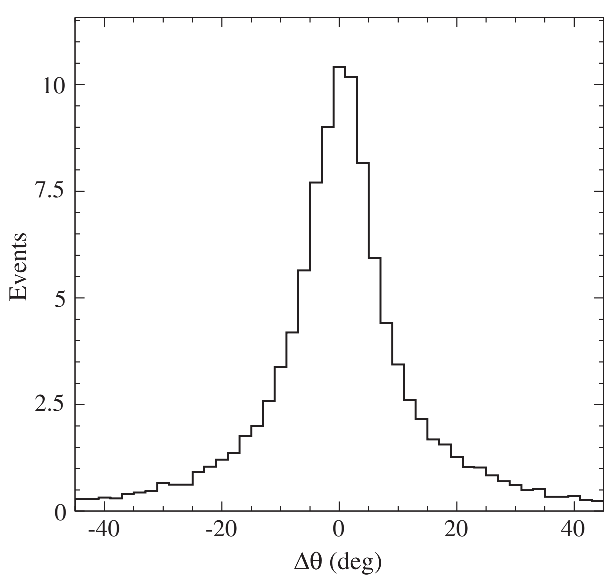

FIG. 6. The distribution of the difference between the true and measured antineutron polar angles at $E_b = 960$ MeV.

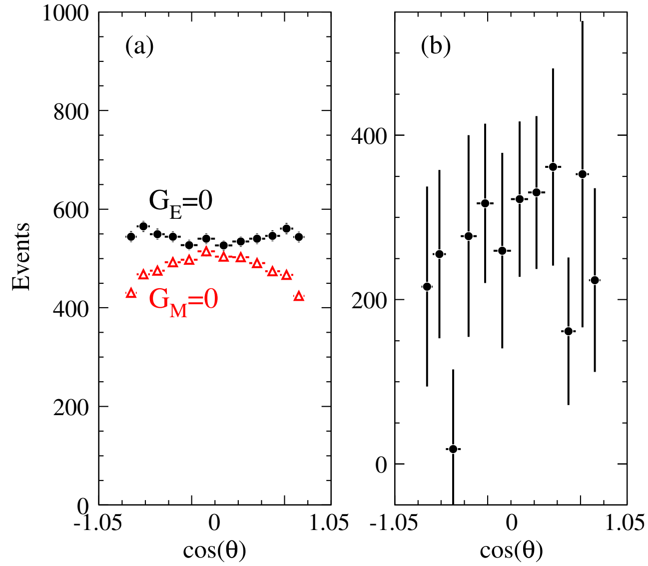

FIG. 7 (color online). (a) The $\cos\theta$ distribution for simulated $e^+e^- \to n\bar{n}$ events generated with $G_E = 0$ and $G_M = 0$. (b) The $\cos\theta$ distribution for data $e^+e^- \to n\bar{n}$ events.

The simulated $\cos\theta$ distributions obtained using the event samples with $G_M = 0$ and $G_E = 0$ are shown in Fig. 7(a). The $\cos\theta$ distribution for data $n\bar{n}$ events is shown in Fig. 7(b). It is seen that the current level of statistics does not allow us to determine the $|G_E/G_M|$ ratio from experiment.

V. CROSS SECTION

The sample of selected $n\bar{n}$ candidates contains a significant fraction, about 70%, of cosmic background events. To separate contributions of cosmic and e^+e^- annihilation events we use a feature of our experiment that data were collected during about 1200 independent runs with different average luminosity ranged from 1×10^{30} to 8×10^{30} cm^{-2} s^{-1}. The number of selected $n\bar{n}$ candidates in the ith run can be written as

$$N_i = xT_i + \sigma_{\rm vis}(E_b)L_i, \tag{4}$$

where x is the cosmic background rate, which is assumed to be constant during the experiment, T_i and L_i are the run duration and integrated luminosity, respectively, and $\sigma_{\rm vis}$ is the visible cross section for the e^+e^- annihilation events that passed our selection, which is a constant for runs belonging to a specific energy point. The system of equations (4) is solved using the maximum-likelihood method independently for the 2011 and 2012 experiments. As a result, we obtain the values of the visible cross section for 7 points below the $n\bar{n}$ threshold and 11 points above.

The values of cosmic rates in 2011 and 2012 are found to be compatible to each other. The average x value is found to be $(1.40 \pm 0.07) \times 10^{-3}$ Hz.

The measured values of $\sigma_{\rm vis}$ are used to obtain the $e^+e^- \to n\bar{n}$ cross section,

$$\sigma_{n\bar{n}} = \frac{\sigma_{\rm vis} - \sigma_{{\rm vis},p\bar{p}} - \sigma_{\rm vis,bkg}}{\varepsilon(1+\delta)}, \quad (5)$$

where ε is the detection efficiency, δ is a radiative correction, $\sigma_{{\rm vis},p\bar{p}}$ is the visible cross section for the $e^+e^- \to p\bar{p}$ events that passed our selection criteria, $\sigma_{\rm vis,bkg}$ is the visible cross section for other background processes. The radiative correction is calculated according to Ref. [10] assuming that the $e^+e^- \to n\bar{n}$ cross section is a constant in the energy region of interest. The systematic uncertainty due to this assumption is estimated to not exceed 2%. The energy dependence of the radiative correction is shown in Fig. 8.

The $e^+e^- \to p\bar{p}$ background contribution is calculated as $\sigma_{{\rm vis},p\bar{p}} = \sigma_{p\bar{p}}\varepsilon_{p\bar{p}}\delta_{p\bar{p}}$, where the Born cross section $\sigma_{p\bar{p}} \approx 0.85$ nb is taken from Ref. [2], the radiative correction $\delta_{p\bar{p}} \simeq \delta$, and the MC detection efficiency $\varepsilon_{p\bar{p}} \approx 0.01\varepsilon$. We estimate the systematic uncertainty on the $p\bar{p}$ contribution to be about 30%.

The background contribution from physical processes other than $e^+e^- \to p\bar{p}$ ($\sigma_{\rm vis,bkg}$) is measured directly below the $n\bar{n}$ threshold. Its value averaged over 7 energy points ranged from $2E_b = 1.8$ to 1.87 GeV is found to be 15 ± 11 pb, about 10% of $\sigma_{\rm vis}$ above threshold. This value is in agreement with the background estimation (10 ± 5 pb) from MC simulation for the processes $e^+e^- \to \gamma\gamma(\gamma)$, $2\pi^0\gamma$, $3\pi^0\gamma$, K_SK_L, $K_SK_L\pi^0$, and $K_SK_L2\pi^0$. To obtain the hadronic cross sections we use the experimental data from Ref. [11] and isotopic relations. In both MC simulation and data we do not observe strong energy dependence of the background cross section. Therefore, the average value of $\sigma_{\rm vis,bkg}$ determined below threshold is taken as an estimate of background above threshold. An additional systematic uncertainty of 10 pb is introduced to account for a possible energy dependence of the background.

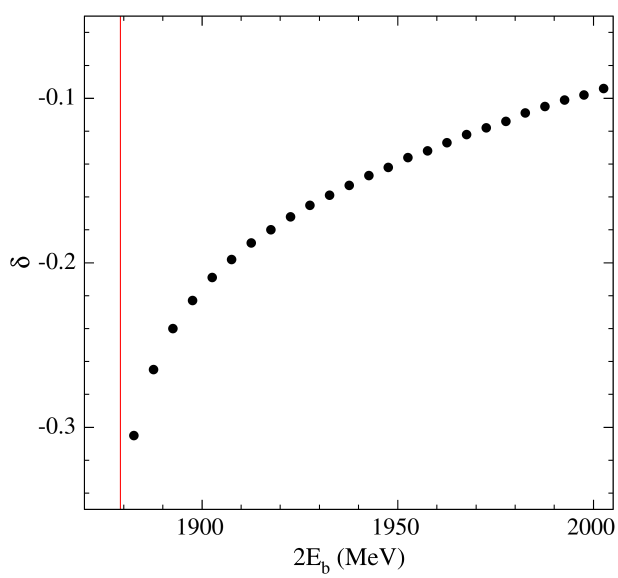

FIG. 8 (color online). The energy dependence of the radiative correction for the $e^+e^- \to n\bar{n}$ process. The vertical line indicates the $n\bar{n}$ threshold.

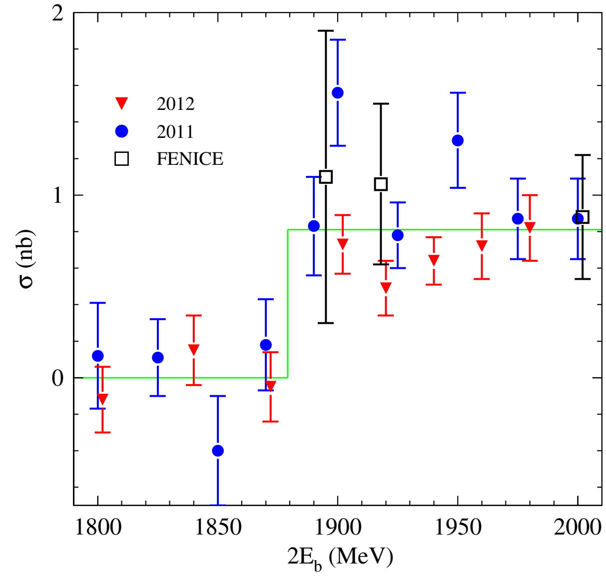

FIG. 9 (color online). The $e^+e^- \to n\bar{n}$ cross section measured in this paper. The filled triangles represent 2011 data, while the filled circles correspond to 2012 data. The FENICE results [4] are shown by the empty squares. The lines below and above the $n\bar{n}$ threshold indicate the average levels of the cross section. The quoted errors are statistical.

The values of the $e^+e^- \to n\bar{n}$ Born cross section obtained using Eq. (5) are listed in Table I and shown in Fig. 9 in comparison with the previous measurement [4]. It

TABLE I. The $e^+e^- \to n\bar{n}$ cross section ($\sigma_{n\bar{n}}$) and neutron effective form factor (F_n) measured in this paper. The quoted errors are statistical. The systematic error is 17% for the cross section and 9% for the form factor.

N	Experiment	$2E_b$, MeV	$\sigma_{n\bar{n}}$, nb	F_n
1	2011	1890	0.83 ± 0.27	0.45 ± 0.09
2	2011	1900	1.56 ± 0.29	0.53 ± 0.06
3	2011	1925	0.78 ± 0.18	0.32 ± 0.04
4	2011	1950	1.30 ± 0.26	0.38 ± 0.04
5	2011	1975	0.87 ± 0.22	0.29 ± 0.04
6	2011	2000	0.87 ± 0.22	0.28 ± 0.04
7	2012	1900	0.73 ± 0.16	0.37 ± 0.06
8	2012	1920	0.49 ± 0.15	0.27 ± 0.06
9	2012	1940	0.64 ± 0.13	0.28 ± 0.04
10	2012	1990	0.72 ± 0.18	0.28 ± 0.05
11	2012	1980	0.82 ± 0.18	0.29 ± 0.05

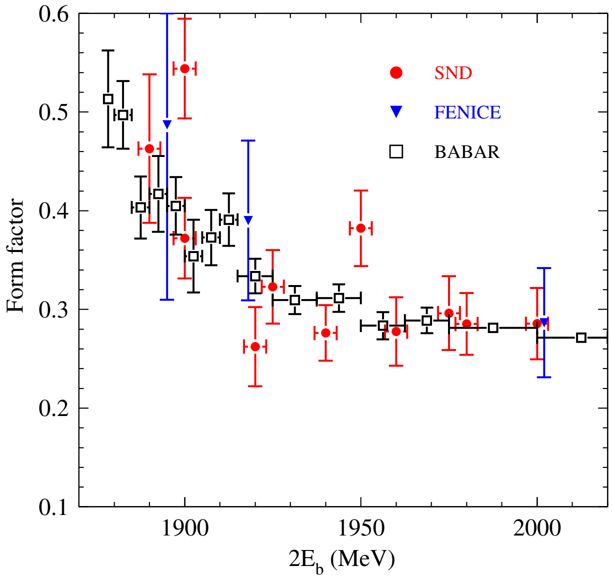

FIG. 10 (color online). A comparison of the neutron effective form factor measured in this paper (SND) and in Ref. [4] (FENICE) and the proton effective form factor measured in the *BABAR* experiment [2].

is seen that our 2011 and 2012 data and the FENICE results are in reasonable agreement.

The systematic uncertainty on the measured cross section includes the uncertainty on the background subtraction (0.05 nb), the uncertainty on the detection efficiency (0.12 nb), the uncertainties in the integrated luminosity (0.02 nb) and the radiative correction (0.02) nb. The total systematic error is 0.14 nb or 17% of the cross section. The error in the cosmic background subtraction (0.12 nb) is included into the statistical error $\sim 25\%$.

The measured $e^+e^- \to n\bar{n}$ cross section has unusual behavior: it is approximately constant in the energy range from threshold up to 2 GeV. Similar behavior in the near threshold region was observed for the $e^+e^- \to p\bar{p}$ cross section [2]. The average $e^+e^- \to n\bar{n}$ cross section below 2 GeV, about 0.8 nb, is close to the average cross section for $e^+e^- \to p\bar{p}$, 0.85 nb.

From the measured cross section we determine the effective neutron form factor [Eq. (3)]. The form-factor energy dependence is shown in Fig. 10 in comparison with the previous FENICE measurements [4], and the proton form-factor data [2]. Both neutron and proton form factors increase near threshold and are close to each other within the measurement errors.

VI. SUMMARY

In the experiment with the SND detector at the VEPP-2000 e^+e^- collider the $e^+e^- \to n\bar{n}$ cross section and the neutron effective form factor have been measured in the c.m. energy range from the $n\bar{n}$ threshold up to 2 GeV. The obtained results are in agreement with the previous FENICE measurements [4] but more precise.

ACKNOWLEDGMENTS

This work is partially supported in the framework of the state order of the Russian Ministry of Science and Education and by RFBR Grants No. 12-02-00065-a, No. 13-02-00375, No. 14-02-31375-mol-a and Scientific School Grant No. 2479.2014.2.

[1] A. B. Arbuzov and T. V. Kopylova, J. High Energy Phys. 4 (2012) 009.
[2] J. P. Lees *et al.* (*BABAR* Collaboration), Phys. Rev. D **87**, 092005 (2013).
[3] G. Bardin *et al.* (PS170 Collaboration), Nucl. Phys. **B411**, 3 (1994).
[4] A. Antonelli *et al.* (FENICE Collaboration), Nucl. Phys. **B517**, 3 (1998).
[5] Yu. M. Shatunov *et al.*, in *Proceedings of the 7th European Particle Accelerator Conference, Vienna, 2000* (EPS, Geneva, 2000), p. 439.
[6] M. N. Achasov *et al.*, Nucl. Instrum. Methods Phys. Res., Sect. A **449**, 125 (2000); **598**, 31 (2009); V. M. Aulchenko *et al.*, *ibid.* **598**, 102 (2009); A. Yu. Barnyakov *et al.*, *ibid.* **598**, 163 (2009); V. M. Aulchenko *et al.*, *ibid.* **598**, 340 (2009).
[7] M. Astrua, E. Botta, T. Bressani, D. Calvo, C. Casalegno, A. Feliciello, A. Filippi, S. Marcello, M. Agnello, and F. Iazzi, Nucl. Phys. **A697**, 209 (2002).
[8] A. V. Bozhenok, V. N. Ivanchenko, and Z. K. Silagadze, Nucl. Instrum. Methods Phys. Res., Sect. A **379**, 507 (1996).
[9] V. F. Dmitriev, A. I. Milstein, and S. G. Salnikov, Phys. At. Nucl. **77**, 1173 (2014).
[10] E. A. Kuraev and V. S. Fadin, Yad. Fiz. **41**, 733 (1985) [Sov. J. Nucl. Phys. **41**, 466 (1985)].
[11] M. N. Achasov *et al.* (SND Collaboration), Phys. Rev. D **88**, 054013 (2013); **90**, 032002 (2014); V. P. Druzhinin, S. I. Eidelman, S. I. Serednyakov, and E. P. Solodov, Rev. Mod. Phys. **83**, 1545 (2011); J. P. Lees *et al.* (*BABAR* Collaboration), Phys. Rev. D **89**, 092002 (2014).